International Journal of Research in Engineering and Science (IJRES)
ISSN (Online): 2320-9364, ISSN (Print): 2320-9356
www.ijres.org Volume 14 Issue 4 ǁ April 2026 ǁ PP. 163-168

Fe-Doped TiO_2 Nanosheets for Efficient Visible-Light Photocatalytic Degradation of Tetracycline

Hongzhao Li[a] *
[a] School of Materials and Chemistry, University of Shanghai for Science and Technology, 516 Jungong Road, Shanghai 200093, P. R. China

Keywords: *Fe-doped TiO_2 nanosheets; visible-light photocatalysis; tetracycline degradation; charge carrier separation; band gap narrowing; oxygen vacancies; photocatalytic mechanism; water treatment*

Date of Submission: 09-04-2026 Date of Acceptance: 22-04-2026

I. Introduction

The contamination of aquatic environments by antibiotic pollutants has become a growing global concern due to their persistence, bioaccumulation, and potential to induce antimicrobial resistance. Among these emerging contaminants, tetracycline (TC) is one of the most widely used broad-spectrum antibiotics in human medicine, livestock production, and aquaculture. Owing to its extensive consumption and incomplete metabolism, considerable amounts of TC are continuously discharged into natural water systems, where it poses serious risks to ecosystems and public health. Therefore, the development of efficient and sustainable technologies for TC removal is of great environmental significance.

Semiconductor photocatalysis has been widely regarded as a promising strategy for the elimination of refractory organic pollutants because it can utilize solar energy to drive redox reactions under mild conditions[1, 2]. In principle, photocatalysts absorb incident photons to generate electron–hole pairs, which subsequently migrate to the surface and participate in interfacial reactions, leading to the decomposition of pollutants[3, 4]. However, the practical photocatalytic efficiency of many semiconductor materials is still limited by several intrinsic drawbacks, including insufficient visible-light absorption, rapid recombination of photogenerated charge carriers, and the lack of efficient active sites for surface reactions[5]. Therefore, rational modulation of the electronic structure and surface chemistry of semiconductor photocatalysts is essential for improving their performance.

TiO_2 is one of the most extensively investigated reducible metal oxides because of its excellent chemical stability, low toxicity, low cost, and strong oxidation capability[6]. In addition to its favorable physicochemical properties, TiO_2 can tolerate defect engineering and elemental doping, making it a versatile platform for photocatalytic applications[7]. Nevertheless, pristine TiO_2 generally suffers from a wide band gap and fast charge recombination, which severely restrict its utilization of visible light and photocatalytic efficiency[8]. In recent years, defect regulation and transition-metal doping have been considered effective strategies to overcome these limitations. In particular, oxygen vacancies, as one of the most common defects in reducible metal oxides, can strongly influence the electronic structure, charge transport behavior, surface reactivity, and oxygen activation ability of TiO_2[9]. The introduction of oxygen vacancies can narrow the band structure-related transition energy, promote carrier separation, and provide additional reactive sites, thereby enhancing photocatalytic activity.

Among various dopants, Fe has attracted considerable attention because of its unique role in simultaneously regulating the lattice structure and electronic properties of TiO_2. When Fe ions are introduced into the TiO_2 lattice, the substitution of Ti^{4+} by Fe^{3+} may lead to charge imbalance, which can be compensated by the formation of oxygen vacancies. Meanwhile, the difference in ionic radius and valence state between Fe and Ti can induce local lattice distortion, further affecting the reducibility, light absorption behavior, and charge transfer characteristics of TiO_2. As a result, Fe doping not only extends the photoresponse of TiO_2 into the visible-light region, but also facilitates the separation and migration of photogenerated carriers. These defect- and doping-induced structural modifications are highly beneficial for photocatalytic pollutant degradation. At the nanoscale, the regulation effect of Fe doping can be further amplified by morphology engineering. Two-dimensional TiO_2 nanosheets possess shortened charge migration pathways, a high specific surface area, and abundant exposed active sites, which are favorable for interfacial catalytic reactions. More importantly, the ultrathin structure can accommodate lattice distortion and defect formation more effectively than bulk materials,

thereby providing a suitable platform for Fe incorporation and oxygen- vacancy generation. The synergistic combination of Fe doping and nanosheet architecture is therefore expected to optimize the band structure of TiO_2, improve visible-light harvesting, and accelerate charge separation and surface oxygen activation. Based on these considerations, Fe-doped TiO_2 nanosheets were constructed in this work through hydrogen reduction treatment using TiO_2 nanosheets as the precursor and ferric nitrate as the Fe source. The obtained pristine TiO_2 nanosheets and Fe-doped TiO_2 nanosheets were denoted as TINS and TIF, respectively. Their morphology, microstructure, optical absorption, and photoelectrochemical properties were systematically characterized by electron microscopy, atomic force microscopy, UV–vis diffuse reflectance spectroscopy, time-resolved photoluminescence, and Mott–Schottky analysis. The photocatalytic performance of the samples was evaluated by the degradation of tetracycline under visible-light irradiation. Compared with TINS, TIF exhibited substantially enhanced photocatalytic activity and a much higher apparent reaction rate. Combined with band structure analysis, the improved performance is mainly attributed to the narrowed band gap, prolonged carrier lifetime, and more favorable electron transfer process induced by Fe doping. In addition, the degradation pathway is closely associated with the generation of superoxide radicals and the direct oxidation by photogenerated holes. This work provides a simple and effective strategy for defect and electronic structure engineering of TiO_2-based photocatalysts for antibiotic-contaminated wastewater treatment.

II. Materials and Methods

Reagents such as TiO_2, K_2CO_3, and Li_2CO_3 were of 99.9% purity or higher (Rare Metallic Co., Japan). All the other chemicals and solvents were of analytical grade and used without further purification. Ultrapure water (>18 MΩ cm) filtered by a Milli-Q water filtration system was used throughout the experiments.Layered potassium titanate, $K_{0.8}[Ti_{1.73}Li_{0.27}]O_4$, was synthesized via a typical high-temperature solid-state reaction. An intimate mixture of TiO_2, K_2CO_3, and Li_2CO_3 (molar ratio of 10.4:2.4:0.8) was placed into a Pt crucible and was calcined at 1173 K for 20 h in air. The protonated form of $H_{1.07}Ti_{1.73}O_4 \cdot H_2O$ was derived from the obtained $K_{0.8}[Ti_{1.73}Li_{0.27}]O_4$ through acid exchange in a 0.5 $mol \cdot dm^{-3}$ HCl solution at ambient temperature for 7 days (the solution was replaced daily with a fresh one). The product was collected by filtration, washed with a copious quantity of pure water to remove excess acid, and air dried at room temperature. The obtained protonated titanate polycrystals were shaken with a tetrabutylammonium hydroxide solution ($(C_4H_9)_4NOH$; TBAOH), the concentration of which corresponds to a molar ratio of 1:1 with respect to the exchangeable protons in the titanate. The solid-to-solution ratio was 4 g L^{-1}. A colloidal suspension of exfoliated $Ti_{1.73}O_4^{1.07-}$ nanosheets was obtained after shaking for 1 week.

III. Results and Discussion

Figure 1 presents the morphological evolution from the layered titanate precursor to Fe- doped TiO_2 nanosheets (TIF). As shown in Figure 1a, the precursor $K_{0.8}[Ti_{1.73}Li_{0.27}]O_4$ exhibits a bulk-like morphology, indicating the typical stacked structure of layered titanates before exfoliation. After proton exchange, the morphology of $H_{1.07}Ti_{1.73}O_4 \cdot H_2O$ (Figure 1b) changes noticeably, showing partially expanded lamellar features, which suggests that the interlayer ions were successfully replaced by protons and water molecules were introduced into the interlayer space. This structural change is favorable for the subsequent exfoliation process. After Fe incorporation and thermal reduction treatment, the obtained TIF sample shows a distinct sheet-like morphology in the SEM image (Figure 1c), confirming the formation of nanosheet structures. The AFM image in Figure 1d further reveals that TIF consists mainly of ultrathin multilayer nanosheets. To better evaluate the thickness, single-sheet AFM images are shown in Figure 1e and Figure 1f. The corresponding three-dimensional AFM profile (Figure 1f) indicates that the thickness of an individual TIF nanosheet is about 3–4 nm, demonstrating the successful preparation of few-layer TiO_2 nanosheets. The microstructure of TIF was further characterized by TEM. In the low-magnification TEM image (Figure 1g), the nanosheet morphology can be clearly observed, which is consistent with the SEM and AFM results. The high-resolution TEM image (Figure 1h) displays clear lattice fringes with an interplanar spacing of 0.351 nm, which can be indexed to the (101) plane of TiO_2[10]. These results confirm that the Fe-doped sample maintains a well-defined crystalline TiO_2 structure after the reduction process.

Overall, the SEM, AFM, and TEM results demonstrate the successful transformation from bulk layered titanate precursors into few-layer Fe-doped TiO_2 nanosheets with a thickness of approximately 3–4 nm and exposed crystalline TiO_2 (101) facets. Such a thin nanosheet structure is expected to provide shortened charge migration pathways and abundant exposed active sites, which are beneficial for photocatalytic performance.

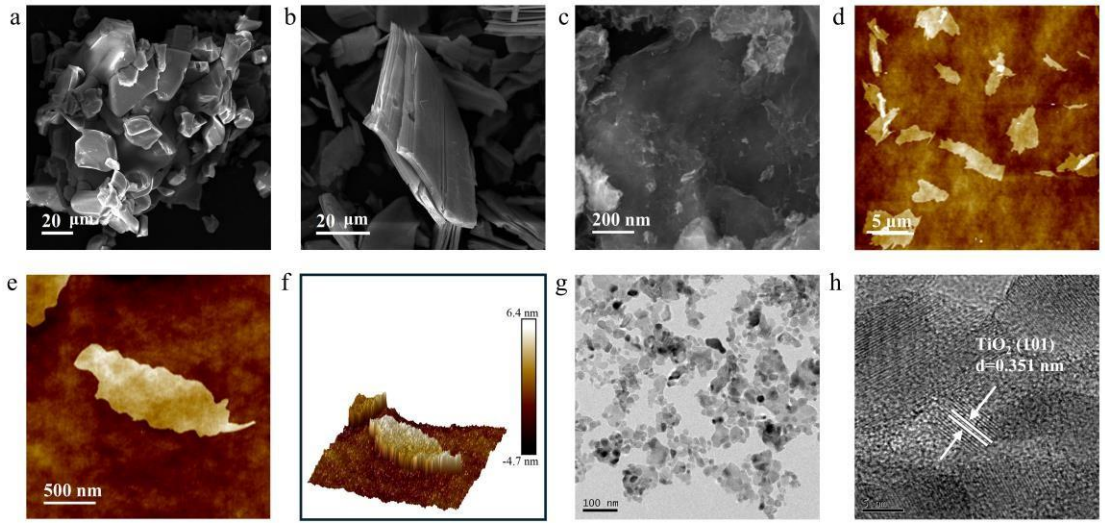

Figure 1. Morphological and structural characterization of the samples during the preparation process. (a) SEM image of $K_{0.8}[Ti_{1.73}Li_{0.27}]O_4$; (b) SEM image of $H_{1.07}Ti_{1.73}O_4 \cdot H_2O$; (c) SEM image of TIF; (d) AFM image of TIF; (e, f) AFM images of an individual TIF nanosheet, where (f) shows the corresponding three-dimensional topographic view; (g, h) low- and high-magnification TEM images of TIF. The lattice fringe spacing of 0.351 nm in (h) corresponds to the TiO_2 (101) plane.

Figure 2 shows the photocatalytic degradation performance of tetracycline (TC) over TINS and TIF. The photocatalytic experiments were carried out using 20 mg of catalyst dispersed in 60 mL of 20 ppm TC solution under light irradiation. As shown in Figure 2a, the degradation efficiency of pristine TiO_2 nanosheets (TINS) is relatively limited, with only 37% of TC removed after 100 min. In contrast, the Fe-doped TiO_2 nanosheets (TIF) exhibit remarkably enhanced photocatalytic activity, achieving 97% degradation within the same reaction time. The significantly improved degradation efficiency indicates that Fe doping plays a critical role in promoting the photocatalytic performance of TiO_2 nanosheets.

To further evaluate the reaction kinetics, the degradation data were fitted using a pseudo-first-order kinetic model. As shown in Figure 2b, the apparent rate constant of TINS is 0.0013 min^{-1}, whereas TIF shows a much higher value of 0.0206 min^{-1}. The kinetic constant of TIF is therefore about 15.8 times higher than that of TINS, confirming its substantially accelerated reaction rate toward TC degradation.

The superior photocatalytic activity of TIF can be attributed to several factors. First, Fe doping effectively narrows the band gap of TiO_2, thereby extending the light absorption range and improving visible-light utilization. Second, the introduced Fe sites can modulate the electronic structure and facilitate the separation and transfer of photogenerated charge carriers, thus suppressing electron–hole recombination. In addition, the ultrathin nanosheet morphology provides short migration pathways for charge carriers and exposes abundant active surface sites. As a result, more reactive species can participate in the degradation of TC, leading to the greatly enhanced photocatalytic efficiency observed for TIF.

These results demonstrate that Fe doping is an effective strategy to improve the photocatalytic degradation performance of TiO_2 nanosheets, enabling rapid and efficient removal of tetracycline from aqueous solution.

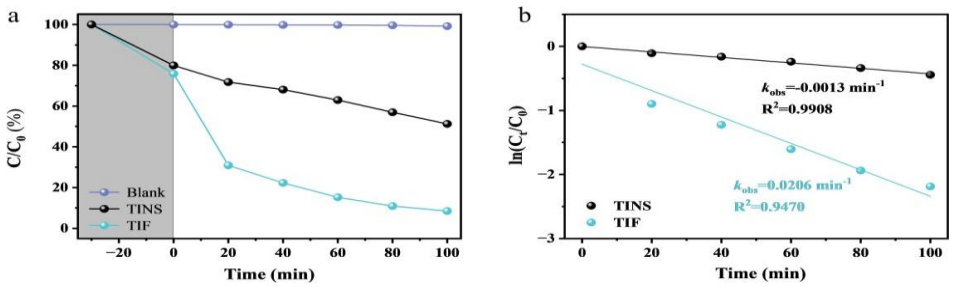

Figure 2. Photocatalytic degradation performance of tetracycline over TINS and TIF.
(a) Photocatalytic degradation curves of tetracycline under light irradiation; (b) pseudo- first-order kinetic fitting plots for tetracycline degradation over TINS and TIF.

To further elucidate the origin of the enhanced photocatalytic activity of TIF, the charge carrier dynamics, band structure, and optical properties were systematically investigated by time-resolved photoluminescence (TRPL), Mott–Schottky (M–S), and UV–vis diffuse reflectance spectroscopy (DRS), as shown in Figure 3.

Figure 3a displays the TRPL decay spectra of TINS and TIF. The average lifetime of TINS is 2.36 ns, while that of TIF increases to 3.06 ns. The prolonged lifetime of photogenerated charge carriers in TIF indicates that Fe doping effectively suppresses the recombination of electrons and holes, thereby promoting charge separation and transfer. This result is consistent with the superior photocatalytic degradation performance of TIF observed in the TC degradation experiments. The semiconductor type and flat-band potentials of the samples were further evaluated by Mott–Schottky analysis (Figure 3b). Both TINS and TIF exhibit positive slopes, confirming their n- type semiconductor nature. The flat-band potentials were determined to be approximately −1.01 eV for TINS and −1.16 eV for TIF (vs Ag/AgCl). Compared with TINS, the more negative flat-band potential of TIF suggests that Fe doping shifts the conduction band to a more negative position, which is beneficial for the reduction of dissolved oxygen to reactive oxygen species, especially $\cdot O_2^-$[11, 12]. This improved reduction ability favors the photocatalytic degradation reaction.

The optical absorption properties of the samples were analyzed by UV–vis DRS. As shown in Figure 3c, the band gap energy of TINS is estimated to be 3.02 eV, whereas that of TIF decreases significantly to 2.35 eV after Fe doping. The narrowed band gap demonstrates that Fe incorporation effectively extends the light absorption edge of TiO_2 from the UV region toward the visible-light region, thus enhancing solar light utilization. Combined with the Mott–Schottky results, the valence band position of TIF is correspondingly shifted to a less positive level compared with that of TINS. Therefore, although Fe doping improves visible-light absorption and electron transfer capability, the valence band potential of TIF is theoretically insufficient to generate $\cdot OH$ from H_2O or OH^-. In contrast, the conduction band position is more favorable for the generation of $\cdot\cdot O_2^-$, indicating that $\cdot O_2^-$ and h^+ are likely the dominant active species in the photocatalytic degradation of tetracycline[13].

Overall, the TRPL, Mott–Schottky, and UV–vis DRS results clearly demonstrate that Fe doping not only broadens the light absorption range of TiO_2 nanosheets by narrowing the band gap, but also enhances charge separation and provides a more suitable band structure for oxygen activation. These synergistic effects account for the greatly improved photocatalytic activity of TIF.

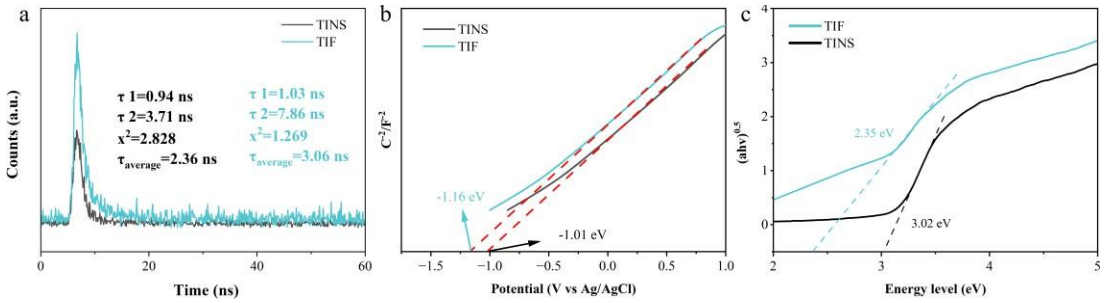

Figure 3. Photophysical and photoelectrochemical properties of TINS and TIF. (a) Time-resolved photoluminescence (TRPL) decay spectra; (b) Mott–Schottky plots; (c) UV–vis diffuse reflectance spectra and corresponding band gap analysis of TINS and TIF.

Based on the photocatalytic performance, TRPL, Mott–Schottky, and UV–vis DRS results, a possible photocatalytic mechanism for tetracycline (TC) degradation over Fe- doped TiO_2 nanosheets (TIF) is proposed, as illustrated in Figure 4. Compared with pristine TiO_2 nanosheets (TINS), Fe doping significantly modifies the electronic structure of TiO_2, resulting in a narrowed band gap from 3.02 to 2.35 eV and a more negative flat-band potential from −1.01 to −1.16 V. As a consequence, TIF exhibits enhanced visible-light absorption and a more favorable band structure for interfacial charge transfer. Under visible-light irradiation, electrons in TIF can be excited from the valence band (VB) to the conduction band (CB), leaving holes in the VB. In addition,

Fe doping introduces impurity or intermediate energy levels in the TiO_2 band structure, which can serve as electron or hole trapping sites. These Fe-related sites help suppress the direct recombination of photogenerated electron–hole pairs and prolong the carrier lifetime, in good agreement with the TRPL results. Therefore, more photogenerated charges can migrate to the catalyst surface and participate in redox reactions. According to the band structure analysis, the CB position of TIF is sufficiently negative to reduce dissolved O_2 to superoxide radicals ($\cdot O_2^-$). These reactive oxygen species can effectively attack tetracycline molecules and initiate a series of degradation reactions. In contrast, the VB position of TIF is not positive enough to efficiently oxidize H_2O or OH^- into hydroxyl radicals (·OH). Therefore, ·OH is unlikely to be the dominant reactive species in this system. Instead, photogenerated holes (h^+) can directly oxidize tetracycline or its intermediate products. Accordingly, $\cdot O_2^-$ and h^+ are considered to be the main active species responsible for TC degradation over TIF[14]. During the photocatalytic process, tetracycline molecules undergo successive oxidative degradation pathways, including demethylation, hydroxylation, ring opening, and chain scission, and are eventually mineralized into small molecules such as CO_2 and H_2O. The excellent photocatalytic activity of TIF can therefore be attributed to the synergistic effects of band gap narrowing, optimized conduction band position, improved visible- light harvesting, and enhanced separation and migration of photogenerated charge carriers induced by Fe doping. Fe doping not only broadens the photoresponse range of TiO_2 nanosheets but also facilitates charge utilization and reactive oxygen species generation, thereby greatly promoting the photocatalytic degradation efficiency of tetracycline.

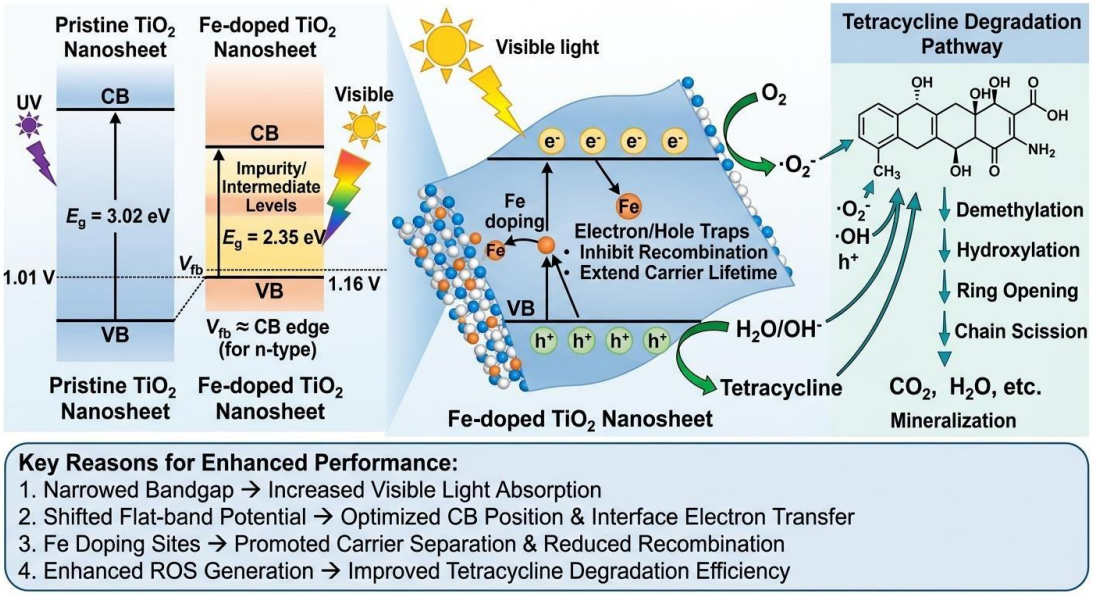

Figure 4. Schematic illustration of the enhanced photocatalytic mechanism of tetracycline degradation over Fe-doped TiO_2 nanosheets. Fe doping narrows the band

gap, shifts the flat-band potential, introduces impurity/intermediate energy levels, and promotes charge separation, thereby facilitating visible-light absorption, superoxide radical generation, and photocatalytic degradation of tetracycline.

IV. Conclusion

In summary, Fe-doped TiO_2 nanosheets (TIF) were successfully prepared through a hydrogen reduction process using TiO_2 nanosheets as the precursor. Compared with pristine TiO_2 nanosheets (TINS), TIF exhibited significantly enhanced photocatalytic activity toward tetracycline degradation. Under the conditions of 20 mg catalyst in 60 mL of 20 ppm tetracycline solution, TIF achieved a degradation efficiency of 97% within 100 min, whereas TINS showed only 37% degradation. The pseudo-first-order rate constant of TIF (0.0206 min^{-1}) was approximately 15.8 times higher than that of TINS (0.0013 min^{-1}). The enhanced photocatalytic performance of TIF can be attributed to the synergistic effects induced by Fe doping. TRPL results revealed a prolonged carrier lifetime, indicating suppressed recombination of photogenerated electron–hole pairs. Mott–Schottky analysis demonstrated that Fe doping shifted the flat-band potential to a more negative value, which is beneficial for oxygen reduction and the generation of superoxide radicals. In addition, UV–vis DRS results showed that the band gap decreased from 3.02 eV for TINS to 2.35 eV for TIF, leading to

improved visible-light absorption. Based on the band structure analysis, $\cdot O_2^-$ and h^+ were identified as the dominant active species in the photocatalytic degradation process. This work demonstrates that Fe doping is an effective strategy for regulating the electronic structure and photocatalytic behavior of TiO_2 nanosheets. The obtained TIF photocatalyst shows great potential for the efficient removal of antibiotic pollutants from water under visible-light irradiation.

References

[1] TAN Y J, SUN R, XU H, et al. Boron-induced spin-polarized defect complexes towards efficient photocatalytic tetracycline decomposition and CO_2 conversion [J]. Applied Catalysis B-Environment and Energy, 2026, 386: 12.

[2] ZHANG S Y, LI X R, MA L, et al. Tailoring reactive oxidative species (ROSs) cascades in a tandem non-thermal plasma/defect-engineered TiO_2 system for enhanced degradation of flotation reagent-laden brine: Unlocking synergistic ROSs generation and pathways [J]. Chemical Engineering Journal, 2026, 529: 16.

[3] ZERJAV G, MAVRIC A, NéMETH M, et al. Support-dependent charge transfer and ROS pathways in Pt/g-C_3N_4 and Pt/ TiO_2 photocatalysts [J]. Chemical Engineering Journal, 2026, 533: 19.

[4] WANG Y T, SHEN G Q, ZHANG Y X, et al. Visible-light-induced unbalanced charge on NiCoP/TiO_2 sensitized system for rapid H_2 generation from hydrolysis of ammonia borane [J]. Applied Catalysis B-Environmental, 2020, 260: 7.

[5] SAADATI A, HABIBI-YANGJEH A, KHATAEE A. A facile synthesis of S-scheme TiO_2-x/$FeTiO_3$ heterojunction photocatalyst for multifunctional hazardous pollutants degradation [J]. Journal of Alloys and Compounds, 2026, 1063: 15.

[6] WEI H T, LI L N, LENG C Y, et al. Construction of Au-Ni bimetallic co-catalysts on TiO_2 for photocatalytic CO_2 reduction to C_2H_6 [J]. Journal of Alloys and Compounds, 2026, 1060: 9.

[7] WANG X G, SUN M H, MURUGANANTHAN M, et al. Electrochemically self-doped WO_3/TiO_2 nanotubes for photocatalytic degradation of volatile organic compounds [J]. Applied Catalysis B-Environmental, 2020, 260: 11.

[8] LI X Y, WANG Y H, MA Y X, et al. TiO_2/$BiVO_4$ photocatalyst based on S-scheme charge transfer and hierarchical porous structure: Efficient ibuprofen degradation and pathway analysis [J]. Journal of Alloys and Compounds, 2026, 1051: 14.

[9] LI Y J, FU Y Z, ZHU M S. Green synthesis of 3D tripyramid TiO_2 architectures with assistance of aloe extracts for highly efficient photocatalytic degradation of antibiotic ciprofloxacin [J]. Applied Catalysis B-Environmental, 2020, 260: 9.

[10] WANG J N, ZHAO K H, YAO Y B, et al. Ferromagnetic Fe-TiO_2 spin catalysts for enhanced ammonia electrosynthesis [J]. Nature Communications, 2025, 16(1).

[11] ZHAO Q, GUO Z, WU Z, et al. Boosting Fe(III)/Fe(II) cycling under visible-light- driven TiO2-based membrane with electron-deficient center for wastewater decontamination [J]. Applied Catalysis B: Environment and Energy, 2025, 366.

[12] CAO C, LIN L, QIU Q, et al. Surface hydroxyl-rich BiOCl/TiO_2 and microwave pretreatment synergistically promote photocatalytic degradation of high density polyethylene microplastics [J]. Journal of Colloid and Interface Science, 2025, 227, 119290.

[13] GUO R, ZENG D, XIE Y, et al. Carbon nitride quantum dots (CNQDs)/TiO_2 nanoparticle heterojunction photocatalysts for enhanced ultraviolet-visible-light-driven bisphenol a degradation and H_2 production [J]. International Journal of Hydrogen Energy, 2020, 45(43): 22534-44.

[14] LI Y, LV K, HO W, et al. Hybridization of rutile TiO_2 (rTiO_2) with g-C_3N_4 quantum dots (CN QDs): An efficient visible-light-driven Z-scheme hybridized photocatalyst [J]. Applied Catalysis B: Environmental, 2017, 202: 611-9.